Supporting Information for

Theoretical study of p-block metal-nitrogen-carbon single-atom catalysts for oxygen reduction reaction

Hao Hu,[a] Peng Zhang,*[,b] Bei-Bei Xiao,[c] and Jian-Li Mi*[,a]

[a] *Institute for Advanced Materials, School of Materials Science and Engineering, Jiangsu University, Zhenjiang 212013, China. Email: jlmi@ujs.edu.cn (J.-L. Mi)*

[b] *Key Laboratory for Water Quality and Conservation of the Pearl River Delta, Ministry of Education, Institute of Environmental Research at Greater Bay, Guangzhou University, Guangzhou 510006, China. Email: pengzhang85@foxmail.com (P. Zhang).*

[c] *School of Energy and Power Engineering, Jiangsu University of Science and Technology, Zhenjiang 212003, China.*

Calculation methods

The Gibbs free energy diagrams of ORR on PM-N_4 are calculated using the reversible hydrogen electrode (RHE) model developed by Nørskov et al..[1] Taken RHE as the reference electrode, the chemical potential (μ) of proton-electron pair is equal to that of half a hydrogen molecule:

$$\mu_{H^+} + \mu_{e^-} = \frac{1}{2}\mu_{H_2}$$

at conditions with $U = 0$ V and $P_{H_2} = 1$ bar.

The free energies (G) of each species are calculated as:

$$G = E_{DFT} + E_{ZPE} - TS$$

where the E_{DFT} is the DFT calculated total energy, E_{ZPE} is zero-point energy and S is the entropy at 298 K. Since the exact free energy of OOH, O, OH radicals in the electrolyte

solution is difficult to obtain, the adsorption free energy ΔG_{OOH*}, ΔG_{O*} and ΔG_{OH*} are relative to the free energy of stoichiometrically appropriate amounts of H_2O (l) and H_2 (g), defined as follows:

$$\Delta G_{OOH*} = G_{OOH*} - G_* - (2G_{H_2O} - \frac{3}{2}G_{H_2})$$

$$= (E_{OOH*} - E_* - 2E_{H_2O} + \frac{3}{2}E_{H_2})$$

$$+ (E_{ZPE}(OOH*) - E_{ZPE}(*) - 2E_{ZPE}(H_2O) + \frac{3}{2}E_{ZPE}(H_2))$$

$$- T \times (S_{OOH*} - S_* - 2S_{H_2O} + \frac{3}{2}S_{H_2})$$

$$\Delta G_{O*} = G_{O*} - G_* - (G_{H_2O} - G_{H_2})$$

$$= (E_{O*} - E_* - E_{H_2O} + E_{H_2})$$

$$+ (E_{ZPE}(O*) - E_{ZPE}(*) - E_{ZPE}(H_2O) + E_{ZPE}(H_2))$$

$$- T \times (S_{OOH*} - S_* - S_{H_2O} + S_{H_2})$$

$$\Delta G_{OH*} = G_{OH*} - G_* - (G_{H_2O} - \frac{1}{2}G_{H_2})$$

$$= (E_{OH*} - E_* - E_{H_2O} + \frac{1}{2}E_{H_2})$$

$$+ (E_{ZPE}(O*) - E_{ZPE}(*) - E_{ZPE}(H_2O) + \frac{1}{2}E_{ZPE}(H_2))$$

$$- T \times (S_{OOH*} - S_* - S_{H_2O} + \frac{1}{2}S_{H_2})$$

The reaction free energy (ΔG) of the elementary steps in ORR was calculated as:

$$\Delta G = \Delta E_{DFT} + \Delta E_{ZPE} - T\Delta S + \Delta G_U + \Delta G_{pH}$$

where ΔE_{DFT} is the difference of total energy, ΔE_{ZPE} and ΔS are the differences in the zero-point energy and the change of entropy, T is 298.15 K, $\Delta G_U = -eU$ and $\Delta G_{pH} = pH \times \kappa_B T \ln 10$ are the contributions from the electrode potential (U) and pH value (κ_B is the Boltzmann constant), respectively.[2,3] Since O_2 in the triplet ground state is notoriously poorly described by DFT computations, the free energy of O_2 was derived as:

$$G_{O_2}(g) = 2G_{H_2O}(l) - 2G_{H_2}(g) - 4.92 \text{ eV}$$

The reaction free energy of (1)-(4) for ORR (at $U = 0$ V vs. RHE) can be calculated using the following equations:

$$\Delta G_1 = \Delta G_{OOH*} - 4.92 \text{ eV}$$

$$\Delta G_2 = \Delta G_{O*} - \Delta G_{OOH*}$$

$$\Delta G_3 = \Delta G_{OH*} - \Delta G_{O*}$$

$$\Delta G_4 = -\Delta G_{OH*}$$

The theoretical overpotential η was adopted to determine the ORR activity of PM-N_4 moieties, which was obtained based on the reaction free energies of the four elemental steps as:

$$\eta = \max\{\Delta G_1, \Delta G_2, \Delta G_3, \Delta G_4\}/e + 1.23 \text{ V}$$

The conductor-like screening model (COSMO) was used to simulate the aqueous environment, and the dielectric constant was set to 78.54.[4]

To evaluate the bonding strength between the PM and the substrate, the binding energy E_b is calculated as:

$$E_b = E_{PM-N_4} - E_{N_4} - E_{PM}$$

where E_{N_4} and E_{PM} is the energy of N_4-doped graphene nanosheet (double carbon vacancies) and isolated one PM atom calculated by DFT, respectively. Also, to compare the bonding strength of PM in PM-N_4 moiety and in bulk metal, the cohesive energies in bulk metal (E_{coh}) are also calculated:

$$E_{coh} = \mu_{PM\,(bulk)} - E_{PM}$$

where $\mu_{PM\,(bulk)}$ is the calculated chemical potential of PM atom from the most stable bulk crystal by DFT.

Microkinetic model for polarization curve simulation

Inspired by the previous study of Nørskov et al.,[5] a microkinetic model has been constructed to simulate the ORR polarization curves of PM-N-C using CatMAP code developed by Nørskov's group.[6] The O_2 molecule diffusion, adsorption and electrochemical reduction steps are listed by the following equations:

$$O_2(aq) \underset{k_{-1}}{\overset{k_1}{\rightleftarrows}} O_2(dl)$$

$$O_2(dl) + * \underset{k_{-2}}{\overset{k_2}{\rightleftarrows}} O_2*$$

$$O_2* + H^+ + e^- \underset{k_{-3}}{\overset{k_3}{\rightleftarrows}} OOH*$$

$$OOH* + H^+ + e^- \underset{k_{-4}}{\overset{k_4}{\rightleftarrows}} O* + H_2O$$

$$O* + H^+ + e^- \underset{k_{-5}}{\overset{k_5}{\rightleftarrows}} OH*$$

$$OH* + H^+ + e^- \underset{k_{-6}}{\overset{k_6}{\rightleftarrows}} O* + H_2O$$

Rate equations

Based on the above reaction steps, the rate equations of each species are accordingly given below:

$$\frac{\partial x_{O_2(dl)}}{\partial t} = k_1 x_{O_2(aq)} - k_{-1} x_{O_2(dl)} - k_2 x_{O_2(dl)} \theta* + k_{-2} \theta_{O_2*}$$

$$\frac{\partial \theta_{O_2*}}{\partial t} = k_2 x_{O_2(dl)} \theta* - k_{-2} \theta_{O_2*} - k_3 \theta_{O_2*} + k_{-3} x_{H_2O} \theta_{OOH*}$$

$$\frac{\partial \theta_{OOH*}}{\partial t} = k_3 \theta_{O_2*} - k_{-3} \theta_{OOH*} - k_4 \theta_{OOH*} + k_{-4} \theta_{O*}$$

$$\frac{\partial \theta_{O*}}{\partial t} = k_4 \theta_{OOH*} - k_{-4} \theta_{O*} - k_5 \theta_{O*} + k_{-5} \theta_{OH*}$$

$$\frac{\partial \theta_{OH*}}{\partial t} = k_5 \theta_{O*} - k_{-5} \theta_{OH*} - k_6 \theta_{OH*} + k_{-6} \theta* x_{H_2O}$$

where x is mole fraction, θ is coverage of the species on one PM site, and *t* is time. x_{H_2O} is taken as 1, and $x_{O_2(aq)}$ is taken as 2.34×10^{-5}, representing to $O_2(g)$ in equilibrium with $O_2(aq)$ at 1 atm. These coverages of the species on one PM site should be satisfied the following condition: $\theta* + \theta_{O_2*} + \theta_{OOH*} + \theta_{O*} + \theta_{OH*} = 1$.

Following the transition state theory, the equilibrium constant (K_i) and the rate constant (k_i) of the non-electrochemical step *i* are given by:

$$K_i = exp\left(-\frac{\Delta G_i}{k_B T}\right)$$

$$k_i = \nu_i exp\left(-\frac{E_{a,i}}{k_B T}\right)$$

where ΔG_i, ν_i, and $E_{a,i}$ are the free energy change, pre-exponential factor, and activation energy of step *i*, respectively. Moreover, k_B is Boltzmann constant, and T is temperature (298.15 K). The values of ν_i are taken from ref 5.

For the electrochemical step, K_i and k_i are associated with the reaction potential (*U* vs. RHE) and given by:

$$K_i = exp\left(-\frac{e(U - U_i)}{k_B T}\right)$$

$$k_i = A_i exp\left(-\frac{E_{a,i}}{k_B T}\right) exp\left(-\frac{e\beta(U - U_i)}{k_B T}\right)$$

where U_i is the reversible potential of step *i* deduced by $U_i = -\Delta G_i/e$, A_i is the effective pre-exponential factor taken as 1.23×10^9, and β is the symmetric factor taken as 0.5. Since the $E_{a,i}$ values of electrochemical ORR steps are generally small, ranging from 0.10 to 0.26 eV,[7,8] $E_{a,i}$ = 0.26 eV is adopted for all the electrochemical steps of the ORR on PM-N-C sites.

Moreover, the rate constants for all the reverse reactions (k_{-i}), can be deduced by:

$$k_{-i} = \frac{k_i}{K_i}$$

Current density

The current density (j) can be deduced by:

$$j = e\rho TOF_{e^-}$$

where e is the elementary charge and ρ is the surface density of active sites of PM-N-C SACs, which is assumed to be comparable with that of Pt(111), and TOF_{e^-} is the turn over frequency of electrons.

Figures

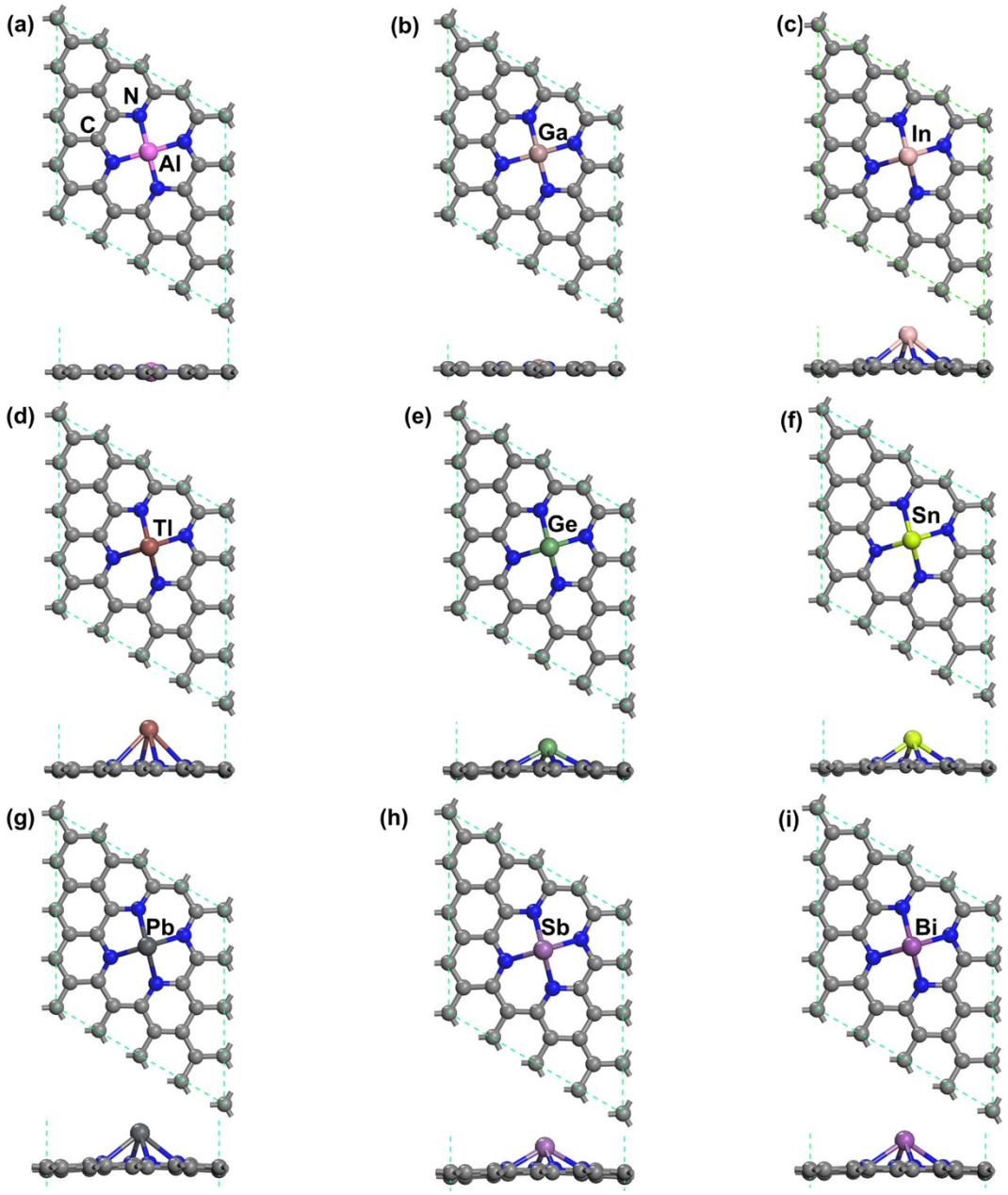

Fig. S1. Optimized 9 geometric configurations of PM-N_4 embedded graphene, containing top view and side view.

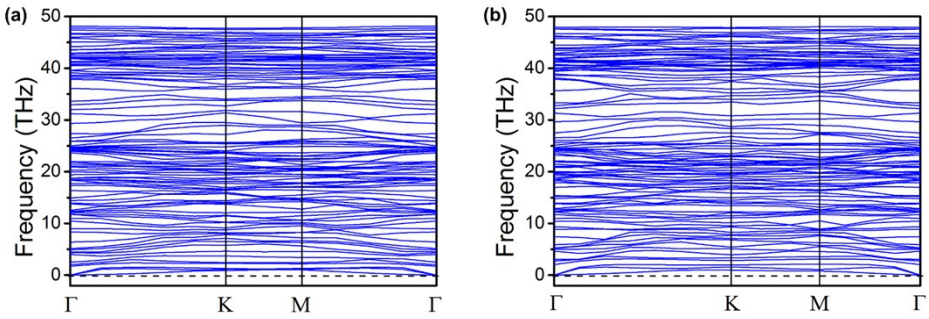

Fig. S2. Phonon dispersion spectra of (a) Tl-N_4 and (b) Pb-N_4.

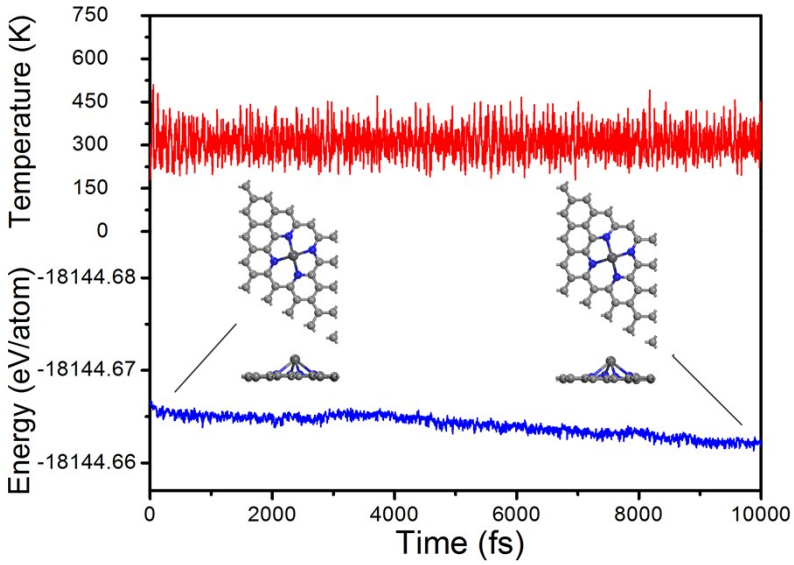

Fig. S3. Evolution of the total energy per atom and the temperature within 10000 fs AIMD simulation at 300 K for Pb-N_4. The inset diagrams show the atomic structure at start and end of the AIMD simulation.

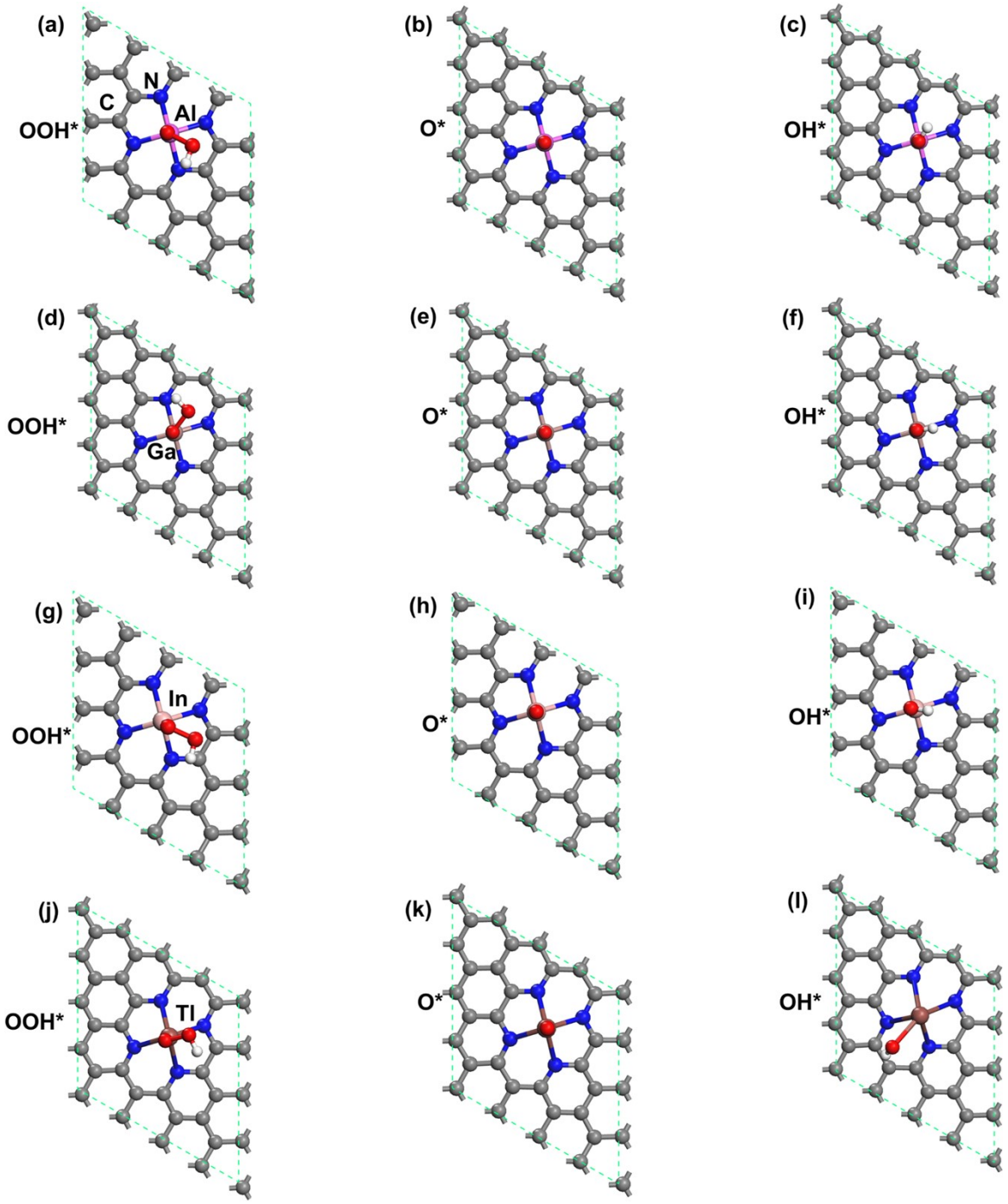

Fig. S4. Optimized adsorption structures of OOH*, O* and OOH* on Al-N_4, Ga-N_4, In-N_4 and Tl-N_4 sites (Grey, blue, red and white spheres represent C, N, O and H atoms, respectively).

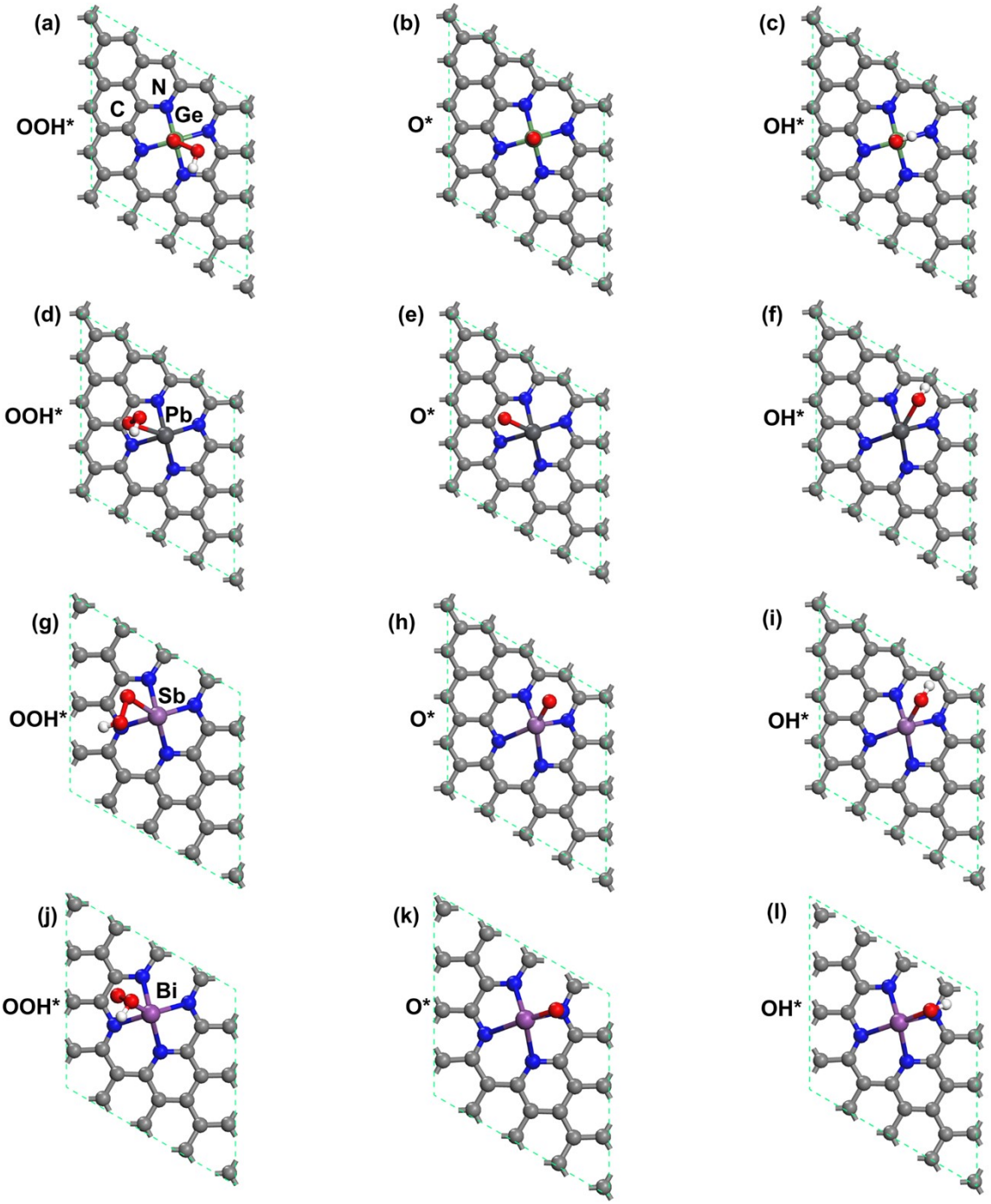

Fig. S5. Optimized adsorption structures of OOH*, O* and OOH* on Ge-N_4, Pb-N_4, Sb-N_4 and Bi-N_4 sites (Grey, blue, red and white spheres represent C, N, O and H atoms, respectively).

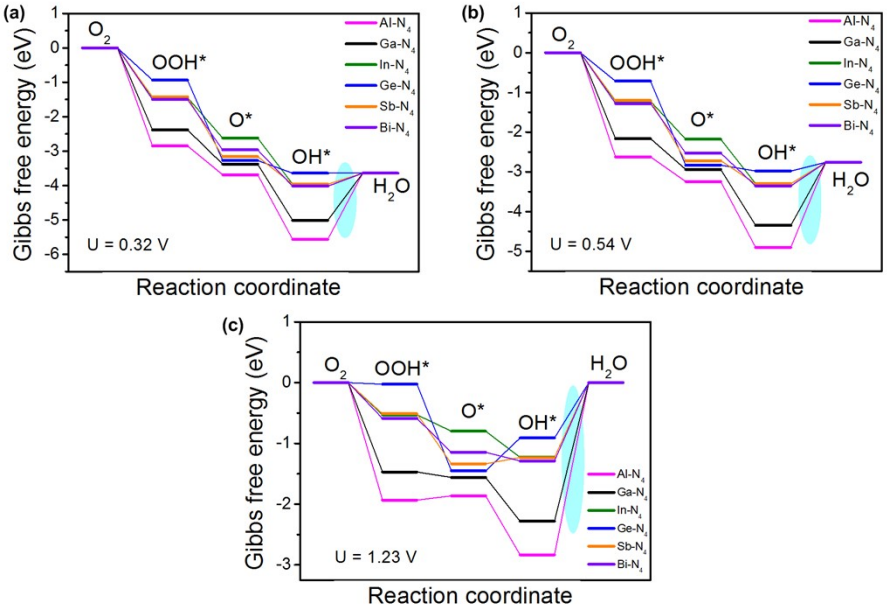

Fig. S6. Reaction free energy profiles of the ORR on PM (Al, Ga, In, Ge, Sb and Bi)-N_4 sites at different potentials.

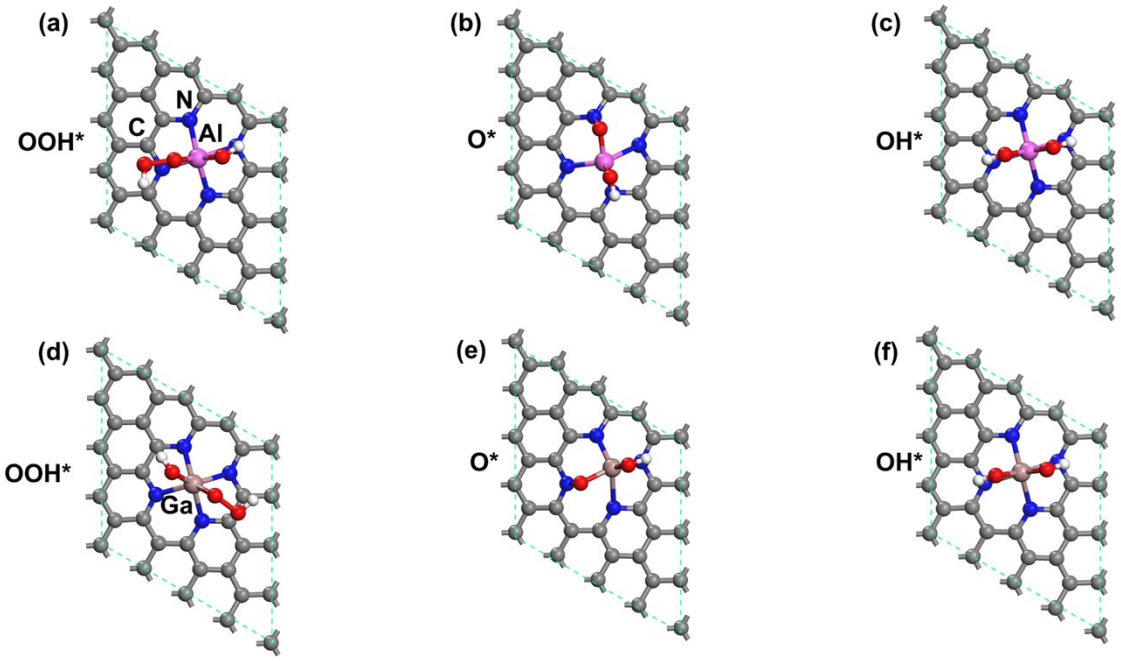

Fig. S7. Optimized adsorption structures of OOH*, O* and OOH* on Al-N_4-OH* and Ga-N_4-OH* (Grey, blue, red and white spheres represent C, N, O and H atoms, respectively).

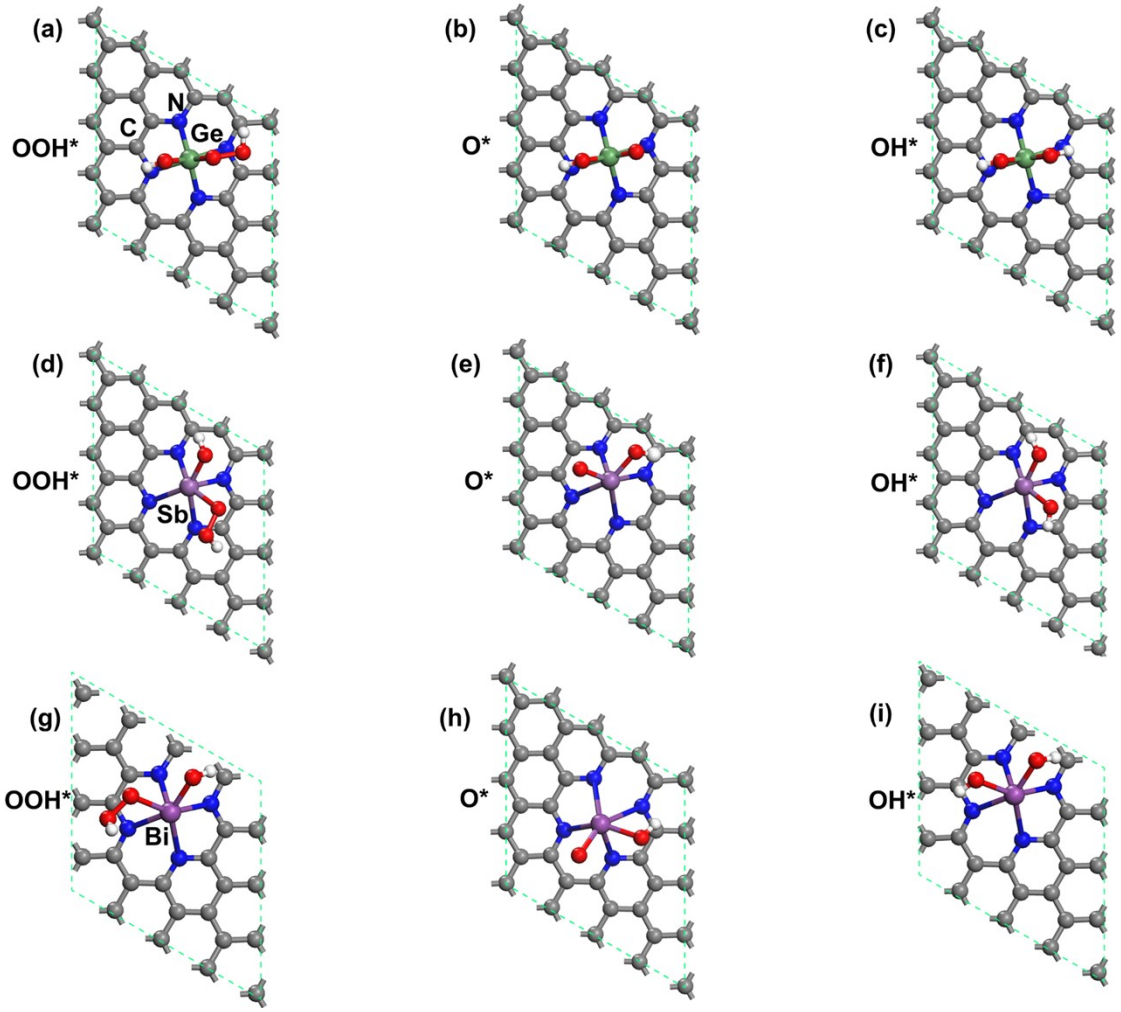

Fig. S8. Optimized adsorption structures of OOH*, O* and OOH* on Ge-N_4-OH*, Sb-N_4-OH* and Bi-N_4-OH* (Grey, blue, red and white spheres represent C, N, O and H atoms, respectively).

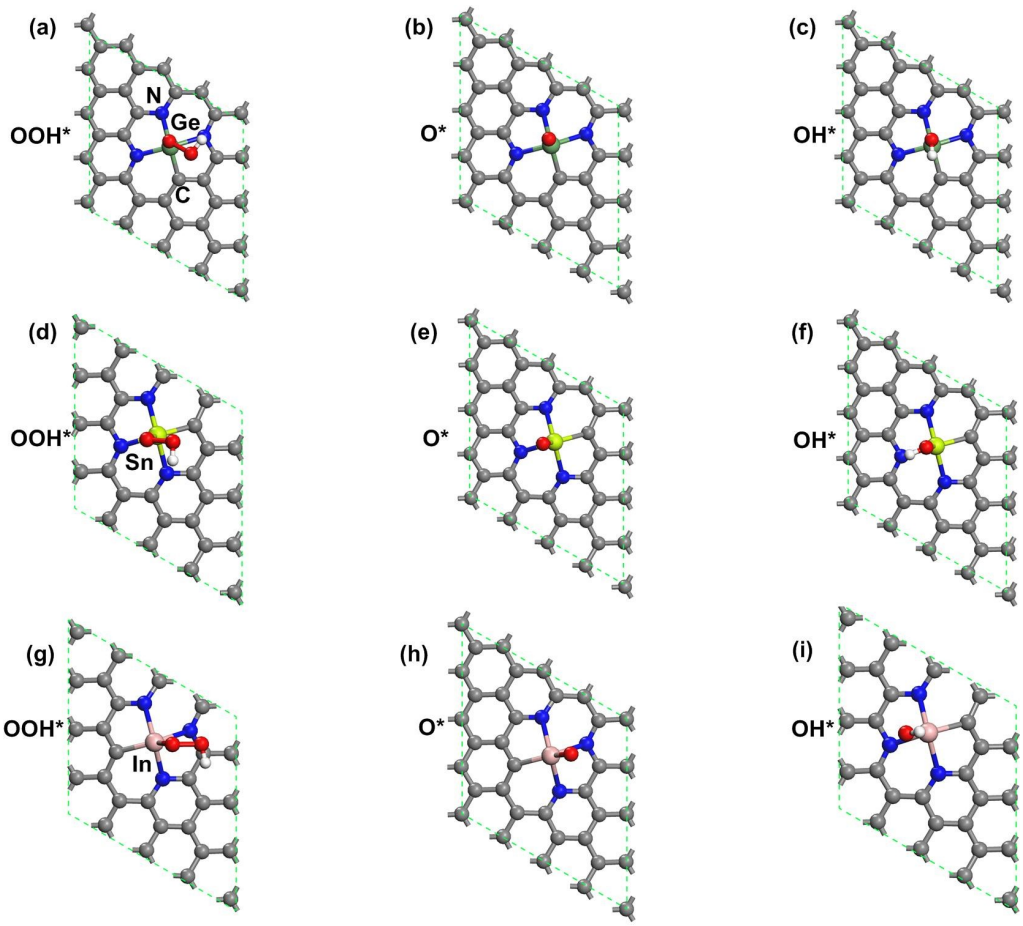

Fig. S9. Optimized adsorption structures of OOH*, O* and OOH* on Ge-N_3C, Sn-N_3C and In-N_3C (Grey, blue, red and white spheres represent C, N, O and H atoms, respectively).

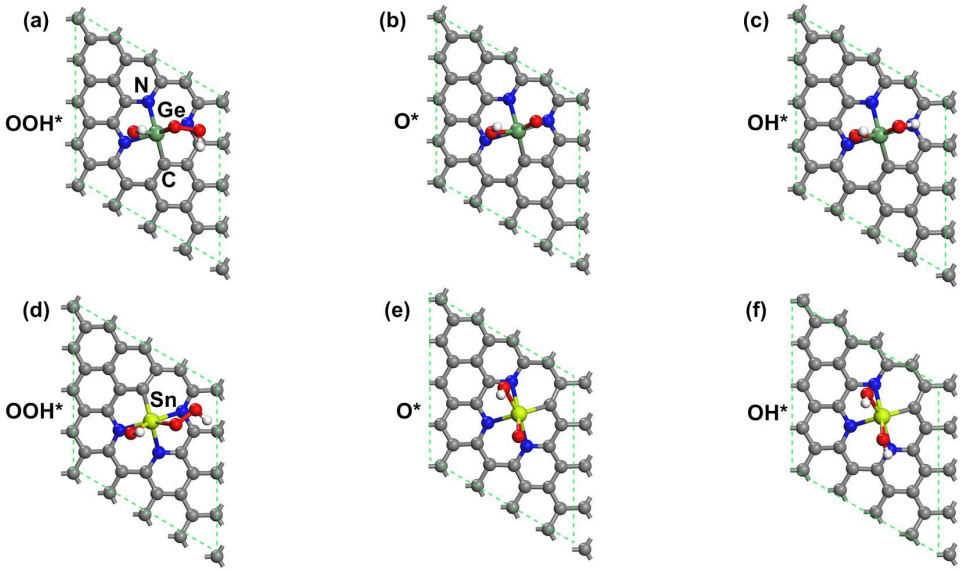

Fig. S10. Optimized adsorption structures of OOH*, O* and OOH* on Ge-N_3C-OH* and Sn-N_3C-OH* (Grey, blue, red and white spheres represent C, N, O and H atoms, respectively).

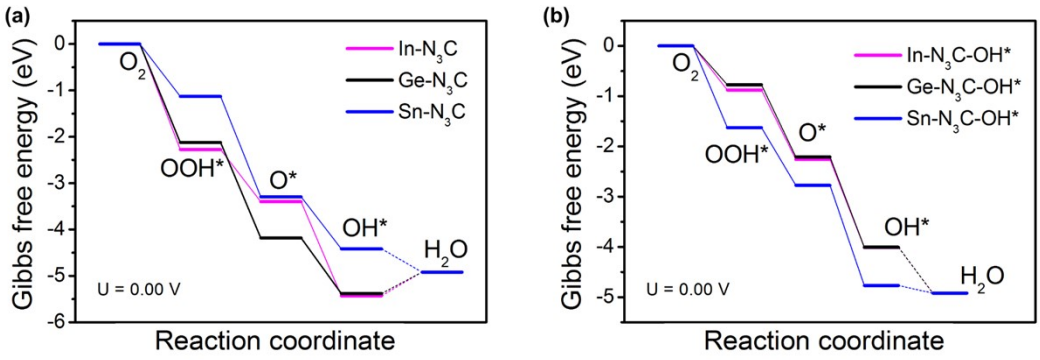

Fig. S11. Reaction free energy profiles of the ORR on the three (a) PM-N_3-C and (b) PM-N_3-C-OH* sites at U = 0 V vs. RHE.

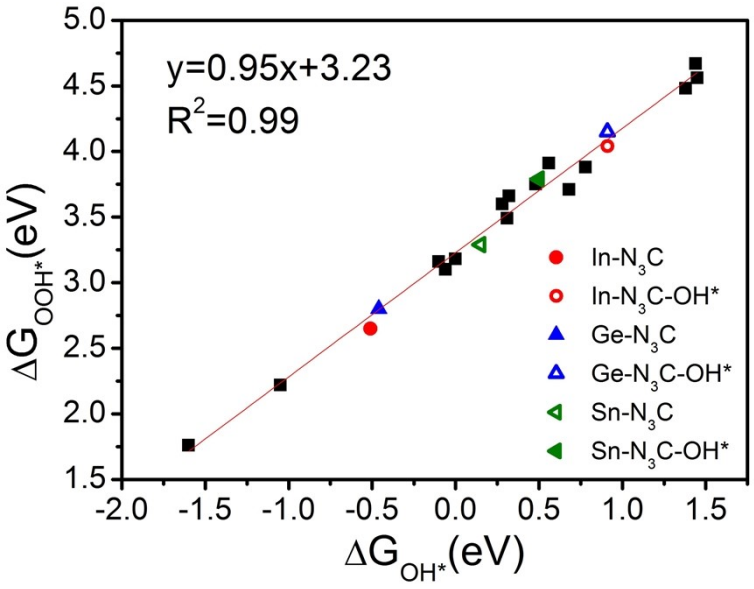

Fig. S12. The linear relationship between ΔG_{OOH*} and ΔG_{OH*} on typical pristine and OH* self-modified PM-N_3-C sites (black dots represent pristine and OH* self-modified PM-N_4 sites). The linear relationship between ΔG_{OOH*} and ΔG_{OH*} for typical PM-N_3-C and PM-N_3-C-OH* sites is consistent with that for PM-N_4 and PM-N_4-OH* sites.

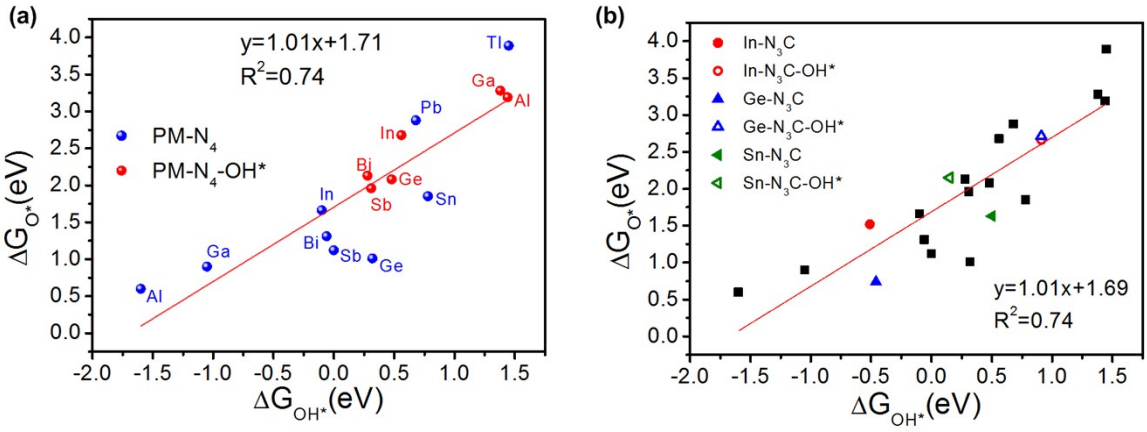

Fig. S13. (a) The linear relationship between ΔG_{O*} and ΔG_{OH*} for pristine and OH* self-modified PM-N_4 sites. (b) The linear relationship between ΔG_{O*} and ΔG_{OH*} for typical pristine and OH* self-modified PM-N_3-C sites (black dots represent pristine and OH* self-modified PM-N_4 sites). The ΔG_{O*} values are almost linearly related to the ΔG_{OH*} values, but the linearity (R^2=0.74) is much lower than that of ΔG_{OOH*} (R^2=0.99).

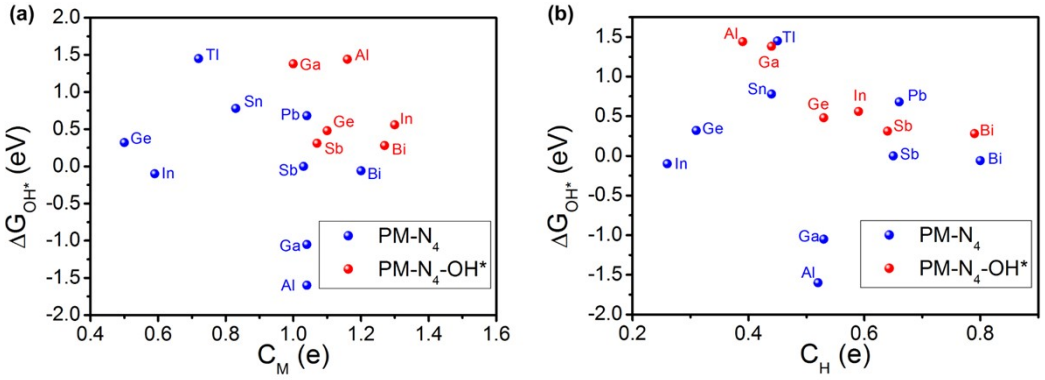

Fig. S14. (a) Mulliken charge (C_M) and (b) Hershfield charge (C_H) of PM atom in PM-N_4 and PM-N_4-OH* sites.

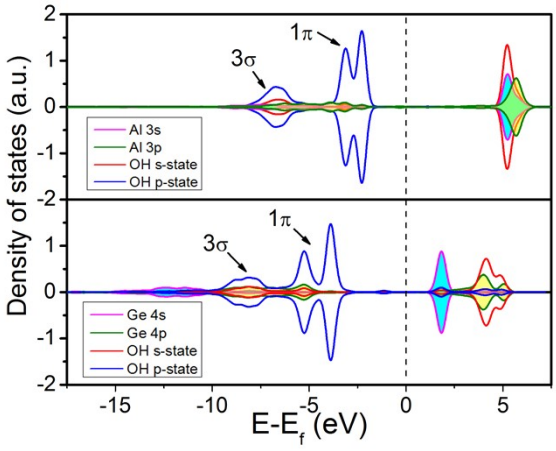

Fig. S15. Density of states (DOS) for OH* adsorbed on Al-N_4 and Ge-N_4. The s-state and p-state of PM atom are depicted by cyan and yellow, respectively.

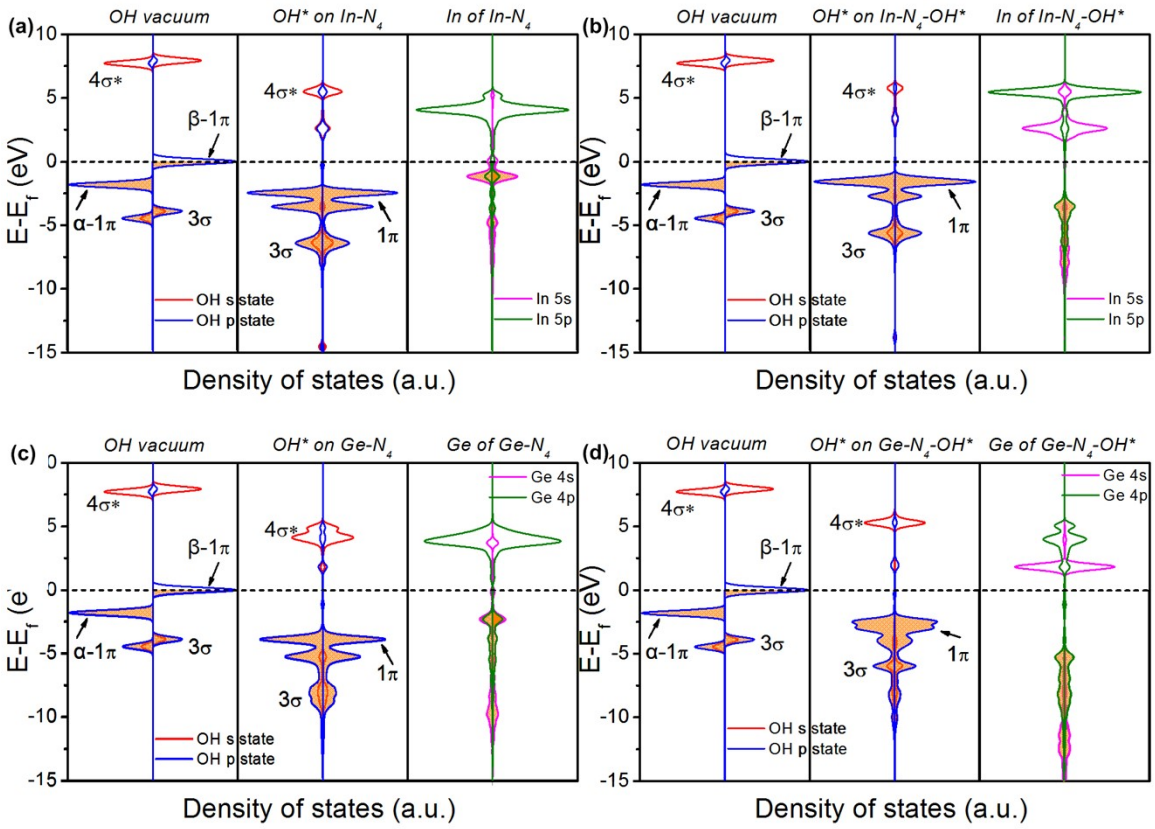

Fig. S16. (a) DOS of vacuum OH and adsorbed OH* on In-N_4 and PDOS of In atom of In-N_4. (b) DOS of vacuum OH vacuum and OH* adsorbed on In-N_4-OH* and PDOS of In atom of In-N_4-OH*. (c) DOS of vacuum OH and adsorbed OH* on Ge-N_4 and PDOS of Ge atom of Ge-N_4. (d) DOS of vacuum OH vacuum and OH* adsorbed on Ge-N_4-OH* and PDOS of Ge atom of Ge-N_4-OH*.

Tables

Table S1. The binding energies (E_b) between Sn and its adjacent N atoms in Sn-N_4 moiety with different orbital cut-off radius (R).

Cut-off energy (Å)	4.6	4.8	5.0	5.2	5.4
Energy (eV)	-4.624	-4.554	-4.527	-4.562	-4.546

Table S2. Convergence test for k-point mesh for the binding energies (E_b) between Sn and its adjacent N atoms in Sn-N_4 moiety.

K-point	2×2×1	3×3×1	4×4×1	5×5×1	6×6×1	7×7×1
Energy (eV)	-4.621	-4.569	-4.562	-4.561	-4.560	-4.559

Table S3. Lattice constants (a×b) of PM-N_4 embedded graphene sheets (c = 20 Å, α = β = 90°, γ = 120°). All results are in unit of $Å^2$.

Al	Ga	In
9.82 × 9.82	9.85 × 9.85	9.82 × 9.82
Tl	Ge	Sn
9.84 × 9.84	9.81 × 9.81	9.84 × 9.84
Pb	Sb	Bi
9.84 × 9.84	9.82 × 9.82	9.84 × 9.84

Table S4. The bond length of PM-N, the height of PM atom above the substrate (h_{PM}), the atomic radii of PM, the binding energy (E_b) between PM and its adjacent N atoms in PM-N_4 moieties, and the cohesive energy (E_{coh}) of PM atom in bulk p-block metal.

PM moiety	PM-N (Å)	h_{PM} (Å)	Atomic radii	E_b (eV)	E_{coh} (eV)
Al-N_4	1.89	0	1.21	-7.36	-3.46
Ga-N_4	1.93	0	1.22	-4.45	-2.73
In-N_4	2.43	1.64	1.42	-3.49	-2.38
Tl-N_4	2.73	2.04	1.45	-2.94	-1.84
Ge-N_4	2.15	1.11	1.20	-5.07	-3.63
Sn-N_4	2.31	1.42	1.39	-4.56	-3.03
Pb-N_4	2.45	1.67	1.46	-3.70	-2.60
Sb-N_4	2.21	1.23	1.39	-2.95	-2.81
Bi-N_4	2.36	1.48	1.48	-1.95	-2.47

Table S5. Values of ΔG_{OOH*}, ΔG_{O*} and ΔG_{OH*} on PM-N_4 embedded graphene.

PM moiety	ΔG_{OOH*} (eV)	ΔG_{O*} (eV)	ΔG_{OH*} (eV)
Al-N_4	1.76	0.60	-1.60
Ga-N_4	2.22	0.90	-1.05
In-N_4	3.16	1.66	-0.10
Tl-N_4	4.56	3.89	1.45
Ge-N_4	3.66	1.01	0.32
Sn-N_4	3.88	1.85	0.78
Pb-N_4	3.71	2.88	0.68
Sb-N_4	3.12	1.12	0.00
Bi-N_4	3.10	1.31	-0.06

Table S6. Reaction free energy of every CPET step and the value of overpotential η for ORR on PM-N_4 sites.

PM moiety	ΔG_1 (eV)	ΔG_2 (eV)	ΔG_3 (eV)	ΔG_4 (eV)	η (V)
Al-N_4	-3.16	-1.16	-2.20	1.60	2.83
Ga-N_4	-2.70	-1.32	-1.95	1.05	2.28
In-N_4	-1.76	-1.50	-1.76	0.10	1.33
Tl-N_4	-0.36	-0.67	-2.44	-1.45	0.87
Ge-N_4	-1.26	-2.65	-0.69	-0.32	0.91
Sn-N_4	-1.04	-2.11	-1.07	-0.78	0.45
Pb-N_4	-1.21	-0.83	-2.20	-0.68	0.55
Sb-N_4	-1.80	-2.00	-1.12	0.00	1.23
Bi-N_4	-1.82	-1.78	-1.37	0.06	1.29

Table S7. Values of ΔG_{OOH*}, ΔG_{O*} and ΔG_{OH*} on PM-N_4-OH* sites.

PM moiety	ΔG_{OOH*} (eV)	ΔG_{O*} (eV)	ΔG_{OH*} (eV)
Al-N_4-OH*	4.67	3.19	1.44
Ga-N_4-OH*	4.48	3.28	1.38
In-N_4-OH*	3.91	2.68	0.56
Ge-N_4-OH*	3.75	2.08	0.48
Sb-N_4-OH*	3.49	1.96	0.31
Bi-N_4-OH*	3.60	2.13	0.28

Table S8. Reaction free energy of every CPET step and the value of overpotential η for ORR on PM-N_4-OH* sites.

PM moiety	ΔG_1 (eV)	ΔG_2 (eV)	ΔG_3 (eV)	ΔG_4 (eV)	η (V)
Al-N_4-OH*	-0.25	-1.48	-1.75	-1.44	0.98
Ga-N_4-OH*	-0.44	-1.20	-1.90	-1.38	0.79
In-N_4-OH*	-1.01	-1.23	-2.12	-0.56	0.67
Ge-N_4-OH*	-1.17	-1.67	-1.60	-0.48	0.75
Sb-N_4-OH*	-1.43	-1.53	-1.65	-0.31	0.92
Bi-N_4-OH*	-1.32	-1.47	-1.85	-0.28	0.95

Table S9. Values of ΔG_{OOH*}, ΔG_{O*} and ΔG_{OH*} on PM (In, Ge, Sn)-N_3C and corresponding PM-N_3C-OH* sites.

PM moiety	ΔG_{OOH*} (eV)	ΔG_{O*} (eV)	ΔG_{OH*} (eV)
In-N_3C	2.65	1.52	-0.51
Ge-N_3C	2.80	0.74	-0.46
Sn-N_3C	3.79	1.63	0.50
In-N_3C-OH*	4.04	2.66	0.91
Ge-N_3C-OH*	4.15	2.71	0.91
Sn-N_3C-OH*	3.29	2.15	0.15

Table S10. Values of $\Delta(\Delta G_{OH^*})$ and ΔG_{OH^*} on PM-N_4 and typical PM-N_3C sites.

PM moiety	$\Delta(\Delta G_{OH^*})$ (eV)	ΔG_{OH^*} (eV)
Al-N_4	3.04	-1.60
Ga-N_4	2.43	-1.05
In-N_4	0.66	-0.10
Ge-N_4	0.16	0.32
Sb-N_4	0.31	0.00
Bi-N_4	0.34	-0.06
In-N_3C	1.42	-0.51
Ge-N_3C	1.37	-0.46
Sn-N_3C	-0.35	0.50

Table S11. Reaction free energy of every CPET step and the value of overpotential η for ORR on typical PM-N_3C and PM-N_3C-OH* sites.

PM moiety	ΔG_1 (eV)	ΔG_2 (eV)	ΔG_3 (eV)	ΔG_4 (eV)	η (V)
In-N_3C	-2.27	-1.13	-2.03	0.51	1.74
Ge-N_3C	-2.12	-2.06	-1.20	0.46	1.69
Sn-N_3C	-1.13	-2.16	-1.13	-0.50	0.73
In-N_3C-OH*	-0.88	-1.38	-1.75	-0.91	0.35
Ge-N_3C-OH*	-0.77	-1.44	-1.80	-0.91	0.46
Sn-N_3C-OH*	-1.63	-1.15	-2.00	-0.15	1.04

Table S12. The Mulliken charge (C_M) and Hershfield charge (C_H) of PM atoms, as well as O highest occupied levels (O_h) of OH* on PM atoms in PM-N_4 sites.

PM moiety	C_M (e)	C_H (e)	O_h (eV)
Al-N_4	1.04	0.52	-1.44
Ga-N_4	1.04	0.53	-1.36
In-N_4	0.59	0.26	-1.63
Tl-N_4	0.72	0.45	0.61
Ge-N_4	0.50	0.31	-2.55
Sn-N_4	0.83	0.44	-0.37
Pb-N_4	1.04	0.66	-0.64
Sb-N_4	1.03	0.65	-1.10
Bi-N_4	1.20	0.80	-0.99

Table S13. The Mulliken charge (C_M) and Hershfield charge (C_H) of PM atoms, as well as O highest occupied levels (O_h) of OH* on PM atoms in PM-N_4-OH* sites.

PM moiety	C_M (e)	C_H (e)	O_h (eV)
Al-N_4-OH*	1.16	0.39	-0.41
Ga-N_4-OH*	1.00	0.44	-0.5
In-N_4-OH*	1.30	0.59	-0.52
Ge-N_4-OH*	1.10	0.53	-1.43
Sb-N_4-OH*	1.07	0.64	-0.61
Bi-N_4-OH*	1.27	0.79	-0.74

References

1 J. K. Nørskov, A. Logadottir and L. Lindqvist, *J. Phys. Chem. B*, 2004, **108**, 17886-17892.

2 L. Yu, X. Pan, X. Cao, P. Hu and X. Bao, *J. Catal.*, 2011, **282**, 183-190.

3 X. M. Zhao, X. Liu, B. Y. Huang, P. Wang and Y. Pei, *J. Mater. Chem. A*, 2019, **7**, 24583-24593.

4 B. Delley, *Mol. Simulat.*, 2006, **32**, 117-123.

5 H. A. Hansen, V. Viswanathan and J. K. Nørskov, *J. Phys. Chem. C*, 2014, **118**, 6706-6718.

6 E. Skúlason, V. Tripkovic, M. E. Bjo¨rketun, S. Gudmundsdo´ttir, G. Karlberg, J. Rossmeisl, T. Bligaard, H. Jo´nsson and J. K. Nørskov, *J. Phys. Chem. C*, 2010, **114**, 18182-18197.

7 V. Tripković, E. Skúlason, S. Siahrostami, J. K. Nørskov and J. Rossmeisl, *Electrochim. Acta*, 2010, **55**, 7975-7981.

8 X. R. Zhu, J. X. Yan, M. Gu, T. Y. Liu, Y. F. Dai, Y. H. Gu and Y. F. Li, *J. Phys. Chem. Lett.*, 2019, **10**, 7760-7766.